Official journal of the JHL 2689-9620
www.light-am.com

Article Open Access

Parallel fabrication of silica optical microfibers and nanofibers

Hubiao Fang[1], Yu Xie[1], Zipei Yuan[1], Dawei Cai[1], Jianbin Zhang[1], Xin Guo[1,2,*] and Limin Tong[1,2,3,*]

Abstract

Optical micro/nanofibers (MNFs) taper-drawn from silica fibers possess intriguing optical and mechanical properties. Recently, MNF array or MNFs with identical geometries have been attracting more and more attention, however, current fabrication technique can draw only one MNF at a time, with a low drawing speed (typically 0.1 mm/s) and a complicated process for high-precision control, making it inefficient in fabricating multiple MNFs. Here, we propose a parallel-fabrication approach to simultaneously drawing multiple (up to 20) MNFs with almost identical geometries. For fiber diameter larger than 500 nm, measured optical transmittances of all as-drawn MNFs exceed 96.7% at 1550-nm wavelength, with a diameter deviation within 5%. Our results pave a way towards high-yield fabrication of MNFs that may find applications from MNF-based optical sensors, optical manipulation to fiber-to-chip interconnection.

Keywords: Parallel fabrication, Fiber tapering, Tensile force, Electric heater, Temperature, Micro/nanofiber

Introduction

Optical micro/nanofibers (MNFs) drawn from standard silica fibers have been widely used as a miniature fiber-optic platform for manipulating optical fields with great versatility[1-3]. Benefitting from their favorable optical properties including low waveguiding loss, strong evanescent fields, tight optical confinement, high power transmission, and excellent compatibility with standard optical fibers[2-5], these MNFs have been extensively studied for applications ranging from optical couplers[6-8], nonlinear optics[9-12], optical sensors[13-16], atom optics[17-19], to fiber lasers[20,21] and opto-mechanics[22-25]. As the structural parameters (waist diameter, uniform length, and tapering profile) of an MNF are subject to different demands in various application scenarios[2,3,26], a number of MNF fabrication and geometry control techniques have been developed[27-32], and MNFs with ultrahigh qualities (e.g., ultra-low loss[33], ultra-high-precision diameter control[30,31,34]) have been realized. However, all these techniques focus on the single-MNF fabrication, that is, drawing one MNF at a time.

In recent years, MNF arrays or multiple MNFs with identical geometries have been attracting more and more attention. Starting from near-field coupling and waveguiding field configuration in two parallel MNFs[35-38], now MNF-array structures have been reported for a variety of applications from efficient single-photon collection[38], compact variable fiber couplers[39], stable atom traps[40], topological phase transitions[41] to high-sensitivity and spatial-resolved optical sensors[36,42,43], and high-resolution compact spectrometers[44]. Moreover, for future industrial

Correspondence: Xin Guo (guoxin@zju.edu.cn) or Limin Tong (phytong@zju.edu.cn)
[1]Interdisciplinary Center for Quantum Information, New Cornerstone Science Laboratory, State Key Laboratory of Extreme Photonics and Instrumentation, College of Optical Science and Engineering, Zhejiang University, Hangzhou 310027, China
[2]Jiaxing Key Laboratory of Photonic Sensing & Intelligent Imaging, Intelligent Optics & Photonics Research Center, Jiaxing Research Institute, Zhejiang University, Jiaxing 314000, China
Full list of author information is available at the end of the article.

applications, high-yield fabrication of MNFs with identical parameters is always desired for large-scale manufacturing MNF-based devices. However, so far, almost all MNF arrays are fabricated with single-MNF fabrication techniques[42,44]. Although the current single-MNF fabrication technique is relatively mature, considering that the low drawing speed (typically 0.1 mm/s) requires a long-term high-precision control and highly stable heating condition, it remains complicated and time-consuming to fabricate a MNF array consisting of multiple MNFs with same geometric parameters.

Here, we demonstrate a parallel-fabrication technique for simultaneously drawing multiple high-quality MNFs in a single step. By investigating and optimizing the drawing force and subsequently the drawing temperature for MNF array fabrication, we have designed and developed a wide-field electric heater that can offer a uniform-temperature distribution (up to 1300 °C) in a 6.2-mm-wide heating zone, and have successfully drawn multiple (up to 20) MNFs with high consistency. Meanwhile, the real-time optical transmittance of each MNF has been measured for in-situ monitoring the drawing process. For typical MNF arrays with diameters from 520 nm to 1.22 μm, the measured optical transmittances of all the as-drawn MNFs exceed 96.7% at 1550-nm wavelength, with a diameter deviation within 5%. Compared with previous single-MNF fabrication techniques, our parallel-fabrication technique, realized by optimizing the heating and drawing conditions, presents a high-yield approach for simultaneously fabricating multiple MNFs with high diameter uniformity and optical transmittance.

Results

Tensile force and working temperature in the MNF tapering process

Similar to that in drawing a standard glass optical fiber[45-47], tensile force and working temperature are critical to yield high-quality optical MNFs. However, unlike that in the standard fiber fabrication, in which the drawing speed can be as high as tens of meters per second (e.g., 25 m/s[48]), a high-transmittance MNF is typically drawn at a much lower speed (e.g., 0.1 mm/s) to facilitate precise shaping of the taper profile to avoid loss from mode transition.

Previously, the tensile force in drawing single MNFs or fiber tapers has been studied[49-52]. Here, the required tensile force increases proportionally with the number of MNFs in the parallel fabrication, and thus may also become an issue to be considered. Fig. 1a shows the schematic diagram of the tensile force measurement system, and the detailed system setup and measurement methods can be found in *Materials and Methods*. Fig. 1b gives the dependence of measured tensile force on the tapering time at typical drawing temperatures from 1140 °C to 1300 °C[53,54], with a fixed drawing speed of 0.1 mm/s. During the drawing process, due to the temperature-dependent viscoelasticity of glass[45,55-57] and the continuously-decreasing diameter of the MNF, the tensile force increases first to the maximum, and then decreases exponentially with tapering time (quadratically with the MNF diameter, see Fig. 1c).

In the parallel fabrication, the maximum tensile force is a crucial consideration. For example, in Fig.1b, when the temperature increases from 1158 °C to 1278 °C, the maximum tensile force for drawing a 20× array of MNFs decreases from 96 N (4.8 N per MNF) to 7.6 N (0.38 N per MNF). The relatively high temperature, and consequently small tensile force are preferred for ensuring the high precision of the mechanical system, such as preventing slipping between the fibers and the clamps, and avoiding over-load operation of the translation stages (e.g., <100 N for Newport M-ILS300LM-S used in this work) for maintaining long-term high precision. On the other hand, excessively high temperature and consequently low viscosity will increase difficulty in controlling the morphology of the tapering region of MNFs. In our system, after optimization, we select a tapering temperature ranging from 1240 °C to 1250 °C for parallel drawing of a 20× fiber array, corresponding to a maximum tensile force of about 15.8 N (at 1250 °C) to 17.4 N (at 1240 °C) (see Fig. S1). By extrapolating the tensile force in Fig.1c, optimizing the fabrication parameters (e.g., tensile force and tapering temperature) for tapering fibers with larger diameters (e.g., > 125 μm) is possible.

In addition, from Fig. 1b, the temperature-dependent maximum tensile pressure can also be obtained (Fig. 1d). The approximately linear dependence of the pressure on the reciprocal of the temperature in the exponential coordinate, agrees well with those reported in drawing standard optical fibers[45,46].

Electric heating scheme

In the initial pulling stage, in order to prevent adjacent glass fibers from sticking together at high temperature, the fibers are arranged in a parallel array at a distance of one fiber apart, thus, a 20× MNF array has a transverse width of about 5 mm. Therefore, compared to the single-MNF drawing case, the parallel fabrication of MNFs requires a high-temperature (e.g., 1250 °C) source that has a much wider zone with uniform-temperature distribution perpendicular to the fiber length, while keeping a similar temperature gradient along the fiber length as the single-MNF case. However, to our knowledge such a heater is not

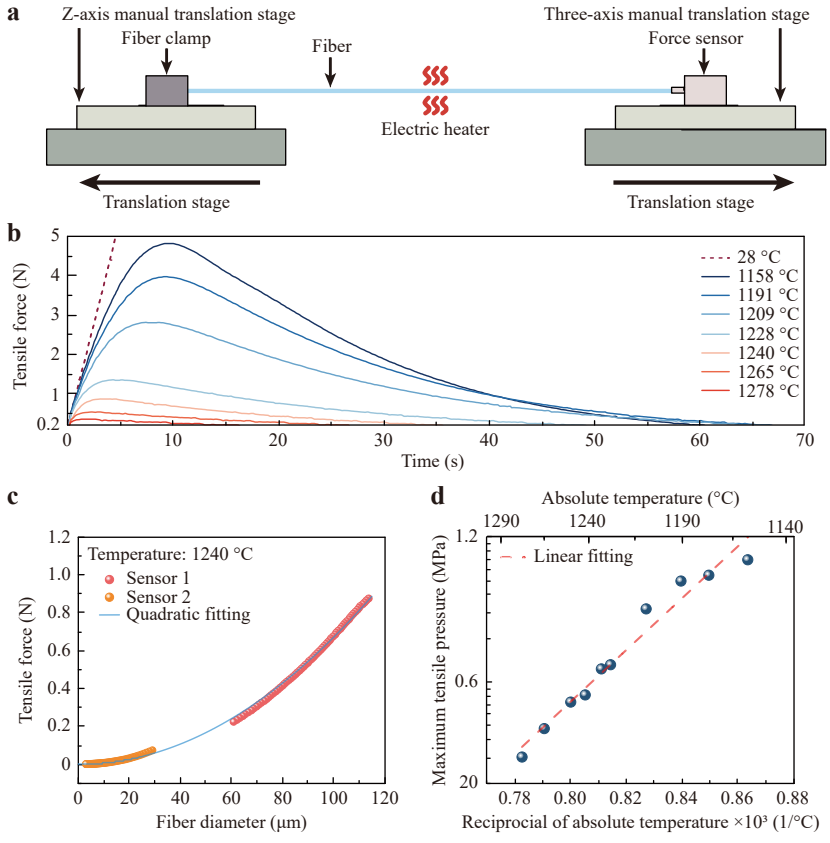

Fig. 1 Tensile force during the tapering process of a single MNF. **a** schematic diagram of MNF tensile force measurement system; **b** tensile force-time curves at different temperatures in the fiber tapering process; **c** tensile force-waist diameter curve at 1240 °C. The red data is measured by a large-range force sensor (ALIYIQI, HF-20), while the orange data is measured by a high-precision force sensor (ME, KD18s±0.1 N). The blue curve is the quadratic function fitted to all the data; **d** relationship between the maximum tensile pressure and temperature. The dashed line is the linear fit of the maximum tensile pressure and reciprocal of the temperature in the exponential coordinate.

yet commercially available.

To satisfy the heating conditions, we design a home-made electric heater. As shown in Fig. 2a, the main heating source is an electric heating wire (FeCrAl alloy) helically wound around two parallel ceramic tubes with a slit size of 3 mm. For thermal insulation, the heater is enclosed by block-shaped polycrystalline mullite fiber boards (not shown here, see more details in Fig. S2). When a proper current is applied on the heating wire, the desired high-temperature field can be generated in the slit. To reduce its oxidation and nitridation, the heating wire is protected by a positive-pressure argon environment (see more details in *Materials and Methods*). Fig. 2b gives a measured temperature distribution on the central plane of the slit (X-Y plane in Fig. 2a) with a current of 8.4 A. It shows that, a 6.2-mm-length uniform temperature distribution (T_{max} = 1243 °C, ΔT < 0.5 °C) along the Y direction is generated (Fig. 2c), with a sharp temperature drop along the X direction.

The long-term-stability test of the heater is also investigated. As shown in Fig. 2d, under a constant current of 8.6 A, the measured maximum temperature gradually increases with the operation time, which can be attributed to the increasing resistance of the heating wire (e.g., from 3.91 to 4.14 Ω after 120 hours), and can be compensated by reducing the current accordingly. When operating at 1250 °C, the measured lifespan of the heater is typically more than 120 hours, close to those of commercial heaters (e.g., NTT CMH-7019) for single-MNF fabrication.

Parallel fabrication of multiple MNFs

Fig. 3a schematically illustrates the experimental setup for parallel fabrication, which is similar to our previous single-MNF pulling system in principle[30,34], except that here the electric heater, the mechanical pulling components and the optical measurement components are designed for multiple fibers (see Fig. S3 for a photograph). The electric heater is fixed on a translation stage for adjusting the

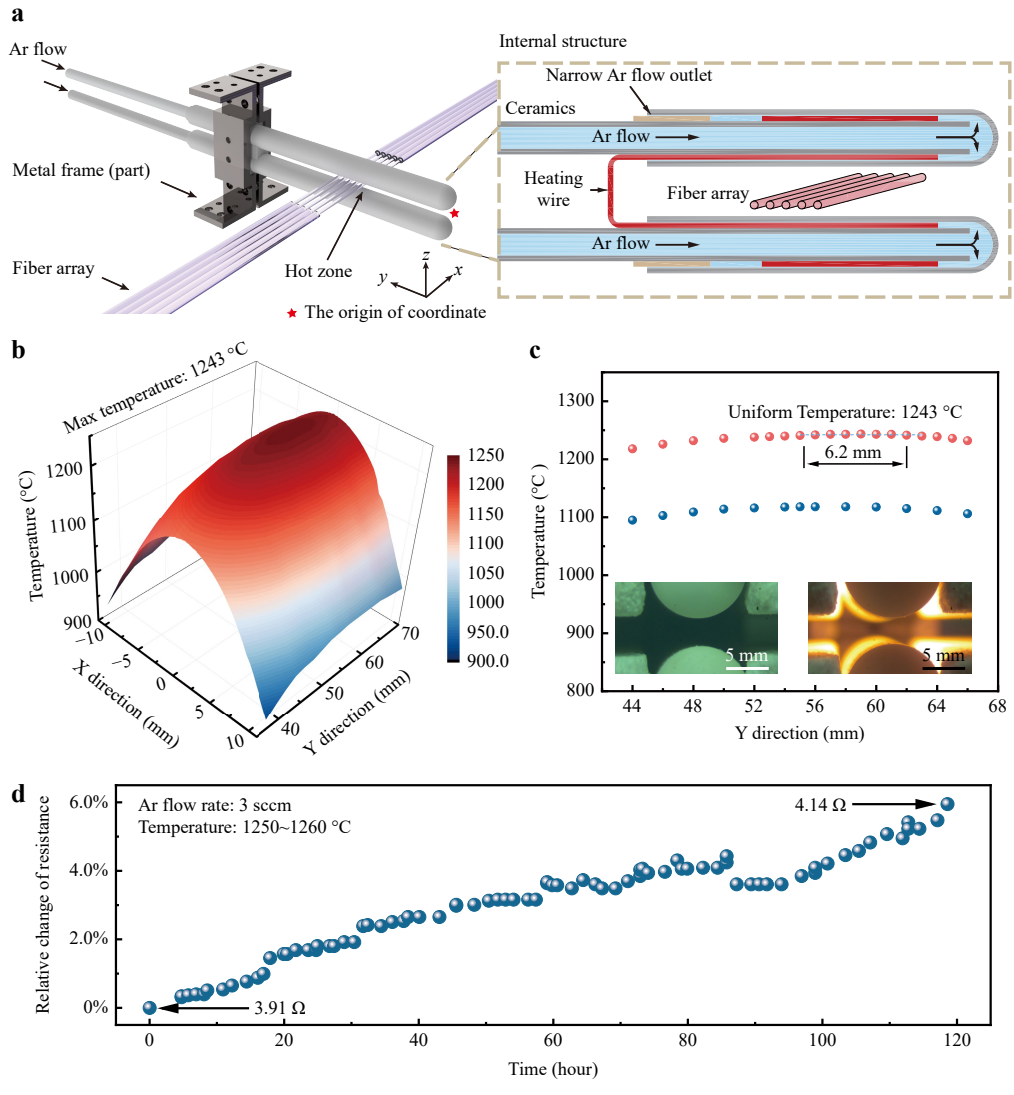

Fig. 2 Fundamental structure and characteristics of the electric heater. **a** schematic diagram of the electric heater. The heating source, that consists of a heating wire (Kanthal, FeCrAl) and ceramic components (e.g., ceramic tubes and sleeves), is supported by the metal frame (6061 aluminum alloy). The block diagram presents a simplified internal structure of the heater. Blue part: Argon gas, red part: heating wire, brown part: ceramic support ring, grey part: ceramic tube. The two electric terminals of heating wire pass through the inner holes of the two ceramic tubes (one from the top and one from the bottom), and are connected to copper wires, which are connected to an external power source through the glass adaptors (see Fig. S2); **b** temperature distribution of the thermal field at the central plane (X-Y plane in Fig. 2a) of the slit; **c** Y-direction temperature distribution of the heater at the central plane of the slit. Pink dots and blue dots are the temperature distribution with the uniform temperatures of 1243 °C and 1117 °C, respectively. Insets, optical photographs of the electric heater at room temperature (23 °C) and working temperature (1243 °C); **d** long-term-stability test of the heater.

relative position between the heater and the fiber array. The fiber clamps (Fig. S4) can fasten up to 20 parallel fibers with a center spacing of around 250 μm (Fig. 3b). The tapering region of the fiber array is in-situ monitored by two cameras from the vertical and horizontal directions, respectively. To monitor the real-time transmittance during the drawing process, a 1550-nm-wavelength light is splitted and coupled into 20 fibers, transmitted through the tapered fibers, and then collected by a 20-channel photodetector (more details in *Materials and Methods*).

Experimentally, the aligned fibers (Corning SMF-28e) are preheated for about 120 seconds at 1240 °C, and then drawn by translation stages that move oppositely at velocities of 0.1 mm/s. Meanwhile, the transmittance of each fiber is measured and recorded at a frequency of 100 Hz, and displayed for real-time monitoring. For example,

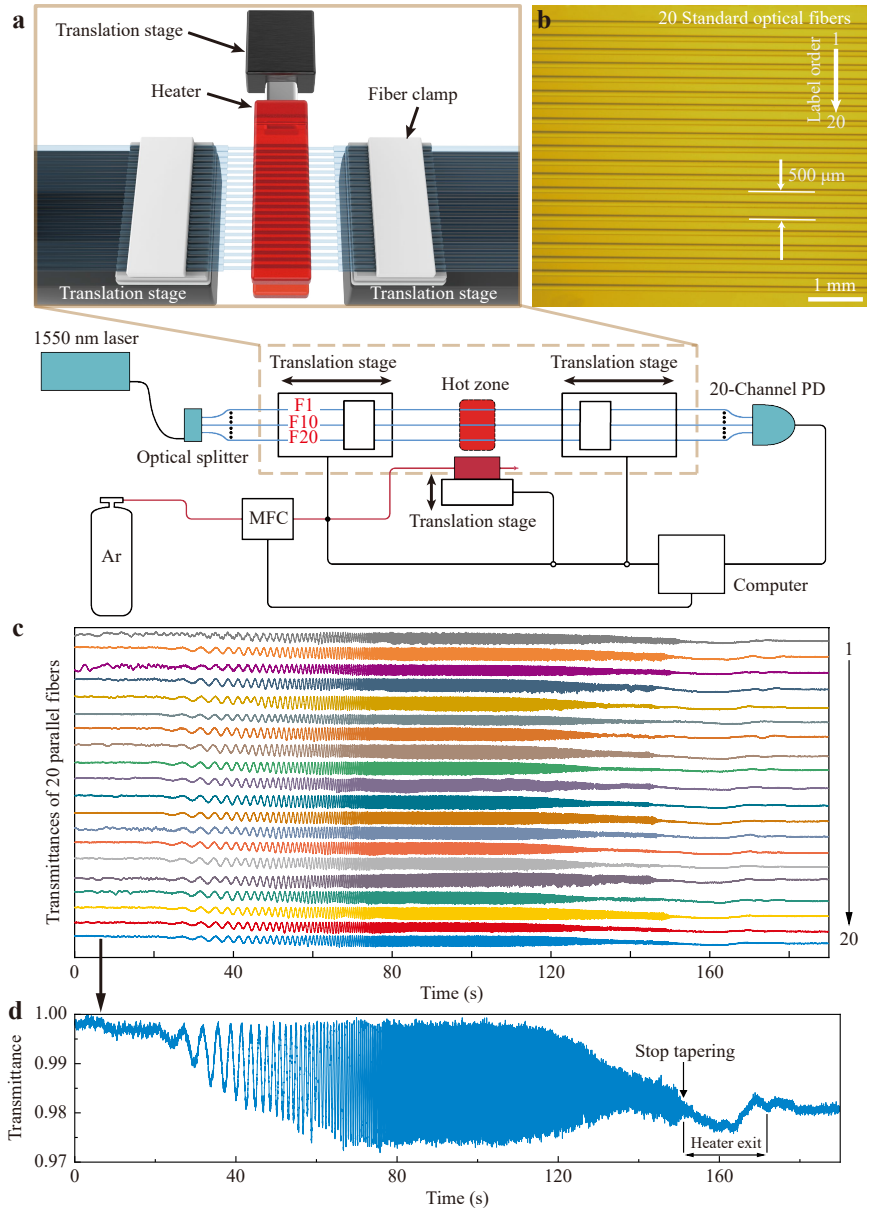

Fig. 3 Parallel-fabrication system. **a** schematic diagram of the parallel-fabrication system for MNFs. The system consists of a home-made electric heater (the red part in the middle), three translation stages (two for fiber tapering, one for heater movement), optical measurement components and a computer. Blue lines represent the fibers and red lines represent the argon gas circuit. Ar, argon gas; PD, photodetector; F, fiber; MFC, mass flow controller; **b** optical image of 20 parallel fibers. These 20 bare optical fibers are fixed on fiber clamps, with a center spacing of about 250 μm; **c** transmittance curves at a wavelength of 1550 nm as functions of time during the tapering process; **d** normalized transmittance of the 20th MNF.

Fig. 3c shows time-dependent transmittances of 20 fibers at a wavelength of 1550 nm. It can be observed that the multimode-induced oscillation for each fiber, which is directly related to the diameter of fibers, starts almost simultaneously and is supressed at approximately the same time, indicating a nearly identical drawing environment of the fibers. For reference, an enlarged transmittance curve of the 20th MNF is shown in Fig. 3d, and a video of typical tapering process can be found in Movie S1. Additionally, fiber arrays can be conveniently dismounted and transferred without fracture by using specially designed transfer tools (see for example, Fig. S5).

Characterization of Parallel-Fabricated MNFs

The optical image of a set of 20 parallel MNFs, corresponding to the transmittance curves (Fig. 3c)

mentioned above, is shown in Fig. 4a. The accurate diameters of the MNFs are measured by scanning electron microscopy (SEM). Fig. 4b shows SEM images of MNFs with the maximum (1.27 μm) and minimum (1.19 μm) diameters within this set of parallel MNFs. Fig. 4c shows the diameters and transmittances of all the 20 MNFs. It can be seen that the diameters are ranging from 1.19 μm to 1.27 μm, with an average diameter of 1.22 μm and a maximum deviation of less than 5%. All the MNFs exhibit a transmittance higher than 97.2%, with the maximum transmittance reaching 99.7%. The excellent diameter uniformity and high transmittance can be maintained for the fabrication of MNF arrays with an average diameter down to about 500 nm, which can be attributed to the high stability of the heating and stretching conditions during the drawing process. For example, Fig. 4d shows the measured diameter and transmittance of an as-fabricated 10× MNF array with a MNF diameter of about 530 nm. Centered around an average diameter of 529.4 nm, the diameters of this set of MNFs are distributed between 519.2 nm and 552.7 nm, with a maximum diameter deviation within 5% and a lowest transmittance of 96.7%. For reference, a typical tapering process of such MNF arrays can be found in Movie. S2. Additionally, fabricating MNF arrays with smaller spacings (e.g., < 125 μm) or large-length uniform waists (e.g., > 10 cm) is challenging with our current parallel-fabrication system. To fabricate such MNF arrays, an improved design for aligning "preform fibers" more densely or a scanning electric heater may be desired.

Discussion

In summary, we have demonstrated a parallel-fabrication approach to simultaneously drawing multiple (up to 20) silica MNFs with high repeatability. Relying on a detailed investigation on the dependence of the tensile force on different tapering temperatures, we optimize the tapering temperature for fabrication of parallel MNFs and have accordingly designed a wide-zone electric heater with a 6.2-mm-width uniform-temperature field. By incorporating the wide-zone electric heater, multi-channel mechanical pulling components and the optical measurement components for multiple fiber drawing, we have fabricated

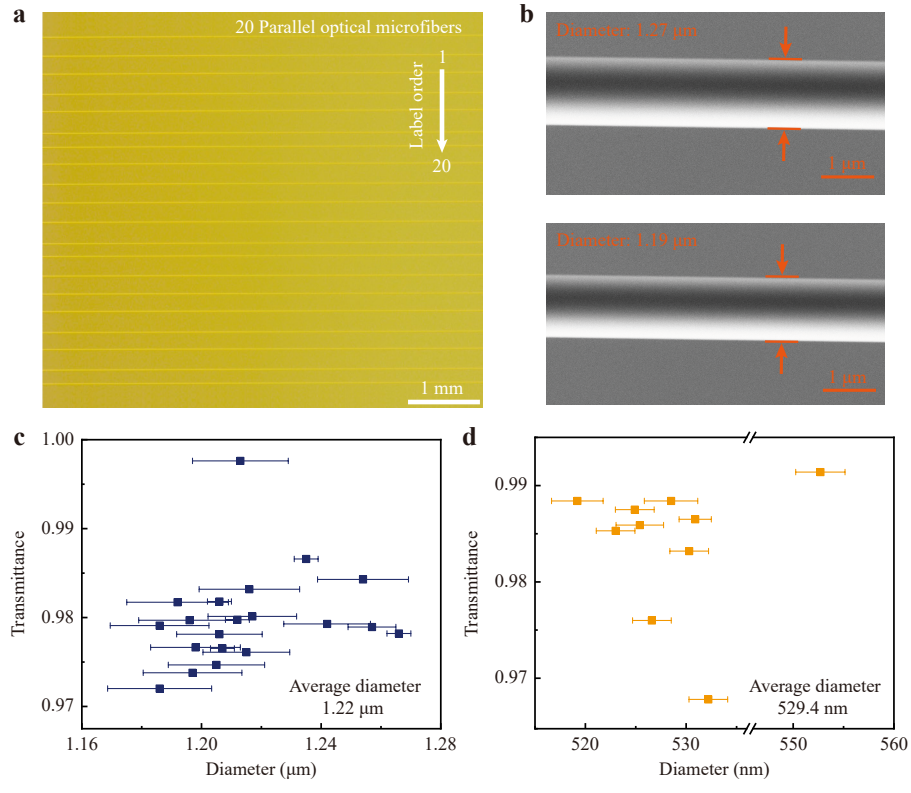

Fig. 4 Characteristics of parallel MNFs. **a** optical image of 20 MNFs in parallel; **b** SEM images of MNFs with the maximum (1.27 μm) and minimum (1.19 μm) diameters within 20 parallel MNFs; **c** diameters and transmittances of 20 parallel MNFs. The diameters are among 1.19 μm to 1.27 μm. The transmittance of each MNF is obtained as the ratio of transmitted power after and before the drawing process, and ranges from 97.2% to 99.7%; **d** diameters and transmittances of 10 parallel MNFs. The diameters are distributed between 519.2 nm and 552.7 nm, and the transmittances range from 96.7% to 99.1%. The error bars are the tolerances of multiple measurements.

MNF arrays with fiber diameters down to ~500 nm. The measured optical transmittances of these MNFs are typically higher than 96.7% at 1550-nm wavelength, with a diameter deviation within 5%. This parallel-fabrication approach can be extended to fabricate fiber arrays with more than 20 fibers. Since MNF arrays are desired in compact variable fiber couplers[39], high-resolution compact spectrometers[44], high-sensitivity and spatial-resolved optical sensors[36,42,43], single-photon collection[38], topological phase transitions[41] and MNF-assisted high-efficiency broadband fiber-to-chip coupling[8], the possibility to fabricate MNF arrays with the excellent diameter uniformity and high transmittance paves a way towards high-yield fabrication of MNFs, which may find broad applications from MNF-based passive optical components, optical sensors, optical manipulation to topological optics and fiber-to-chip interconnection.

Materials and Methods

Tensile force measurement

The tensile force measurement system is shown in Fig. 1a. A 12.5-cm-length standard optical fiber (Corning SMF-28e) with around 6-cm-length coating peered off was used to measure the tensile force of taper-drawn biconical fiber during the drawing process. The both ends of the optical fiber were fixed to a fiber clamp and a force sensor (ALIYIQI, HF-20) on both sides, respectively. The optical fiber, the clamp, and the force sensor were along the same horizontal line by adjusting a Z-axis manual translation stage (DHC, GCM-V25M) and a three-axis manual translation stage (OMTOOLS, OMYE62D) on both sides. The electric heater was used to generate a constant hot zone and heat the fiber to a certain temperature (1140 °C ~ 1300 °C). After the fiber reached a thermally stable state, two translation stages (Newport M-IMS500LM-S) began to taper it at a controlled speed of 0.1 mm/s, respectively, and the force sensor simultaneously measured the tension data during the whole drawing process.

Electric heating scheme for 20 parallel MNFs

A 1-mm-diameter helically wound heating wire (Kanthal, FeCrAl) with a mean coil diameter of 6 mm was used as the heating source. The length of the heating wire can be customized according to the required heating range. For example, a heating wire with a spiral length of 8 cm (40 turns) and a resistance of about 4 Ω was chosen for the parallel fabrication of 20 MNFs.

The heating wire was supported by two parallel ceramic tubes, as the red part in the internal structure (the right panel of Fig. 2a). As mentioned in Section *Electric heating scheme*, the heating source was wrapped by block-shaped polycrystalline mullite fiber boards (see Fig. S2) and can generate high temperature in the 3 mm-wide slit between the ceramic sleeves when energized. Typically, this electric heating source was capable of operating reliably within a temperature range below 1300 °C and the required voltage did not exceed 40 V. Considering the fact that the heating wire has obvious corrosion reaction with the oxygen and nitrogen in the surrounding air under high-temperature circumstances[58,59], e.g., $2Cr + N_2 = 2CrN$ (800 °C ~ 1400 °C), an argon gas environment around the heating wire was applied to reduce its aging rate. As illustrated in Fig. 2a, the ceramic tubes and the ceramic sleeves that supported and protected the heating wire also served to guide the argon gas, where the argon gas flowed through the inner cavity of the ceramic tubes, traversed through the interlayer, and ultimately exited. The notched ceramic rings (brown part in internal structure, Fig. 2a) were positioned at the end of the sleeves, complemented by a few sealants, to effectively minimize the egresses of the gas flow while providing structural support. The flow rate was precisely controlled to 3 sccm by two flow controllers (Sevenstar, CS100), respectively.

Real-time transmittance monitoring

To monitor the transmittance of optical fiber arrays, a 1550-nm-wavelength light (Connet Laser, VLSS1550-B) was evenly split into 20 channels by an optical fiber splitter, which were coupled into optical fibers by ferrule connectors, respectively. A multichannel photodetector used to detect and collect transmittance data was consisted of 20 analog pin detectors, 20 voltage signal amplifiers and a multi-channel data acquisition card (Smacq USB-3131). This multichannel photodetector can collect signals from 20 channels one by one at a maximum sampling frequency of about 12 kHz. As the sampling time τ we used for each channel is 0.5 ms, it costed only 10 ms to complete a round of sampling all the 20 fibers. Compared with the relatively slow drawing speed (0.1 mm/s), the transmittance measurement of the 20 fibers can be approximately regarded as simultaneous.

Acknowledgements

This research was supported by the National Natural Science Foundation of China (62175213 and 92150302), the National Key Research and Development Program of China (2018YFB2200404), the New Cornerstone Science Foundation (NCI202216), the Natural Science Foundation of Zhejiang Province (LR21F050002), and the Fundamental Research Funds for the Central Universities (2023QZJH27). The authors thank Dong Han for suggestions on the processing of fiber clamps, and also thank Wei Wang for her assistance with SEM.

Author details
[1]Interdisciplinary Center for Quantum Information, New Cornerstone Science Laboratory, State Key Laboratory of Extreme Photonics and Instrumentation, College of Optical Science and Engineering, Zhejiang University, Hangzhou 310027, China. [2]Jiaxing Key Laboratory of Photonic Sensing & Intelligent Imaging, Intelligent Optics & Photonics Research Center, Jiaxing Research Institute, Zhejiang University, Jiaxing 314000, China. [3]Collaborative Innovation Center of Extreme Optics, Shanxi University, Taiyuan 030006, China

Author contributions
L.T. and X.G. conceived the idea, designed the experiments, and supervised the research project. H.F., Y.X., Z.Y., D.C., and J.Z. designed and conducted the experiments. H.F. analyzed the data and wrote the paper. All authors participated in the analysis of data and contributed to the writing of manuscript.

Conflict of interest
The authors declare no conflict of interests.

Supplementary information is available for this paper at https://doi.org/10.37188/lam.2024.020.

Received: 29 November 2023 Revised: 20 March 2024 Accepted: 22 March 2024
Accepted article preview online: 23 March 2024
Published online: 08 July 2024

References

1. Tong, L. M. et al. Subwavelength-diameter silica wires for low-loss optical wave guiding. *Nature* **426**, 816-819 (2003).
2. Brambilla, G. et al. Optical fiber nanowires and microwires: fabrication and applications. *Advances in Optics and Photonics* **1**, 107-161 (2009).
3. Wu, X. Q. & Tong, L. M. Optical microfibers and nanofibers. *Nanophotonics* **2**, 407-428 (2013).
4. Tong, L. M., Lou, J. Y. & Mazur, E. Single-mode guiding properties of subwavelength-diameter silica and silicon wire waveguides. *Optics Express* **12**, 1025-1035 (2004).
5. Zhang, J. B. et al. High-power continuous-wave optical waveguiding in a silica micro/nanofibre. *Light:Science & Applications* **12**, 89 (2023).
6. Guo, X. et al. Direct coupling of plasmonic and photonic nanowires for hybrid nanophotonic components and circuits. *Nano Letters* **9**, 4515-4519 (2009).
7. Cai, L., Pan, J. Y. & Hu, S. Overview of the coupling methods used in whispering gallery mode resonator systems for sensing. *Optics and Lasers in Engineering* **127**, 105968 (2020).
8. Jin, Y. Y. et al. Efficient fiber-to-chip interface via an intermediated CdS nanowire. *Laser & Photonics Reviews* **17**, 2200919 (2023).
9. Leon-Saval, S. G. et al. Supercontinuum generation in submicron fibre waveguides. *Optics Express* **12**, 2864-2869 (2004).
10. Beugnot, J. C. et al. Brillouin light scattering from surface acoustic waves in a subwavelength-diameter optical fibre. *Nature Communications* **5**, 5242 (2014).
11. Jiang, B. Q. et al. High-efficiency second-order nonlinear processes in an optical microfibre assisted by few-layer GaSe. *Light:Science & Applications* **9**, 63 (2020).
12. Hao, Z. et al. Broadband and continuous wave pumped second-harmonic generation from microfiber coated with layered GaSe crystal. *Opto-Electronic Advances* **6**, 230012 (2023).
13. Li, H. T. et al. Single-molecule detection of biomarker and localized cellular photothermal therapy using an optical microfiber with nanointerface. *Science Advances* **5**, eaax4659 (2019).
14. Cao, Z. X. et al. Biochemical sensing in graphene-enhanced microfiber resonators with individual molecule sensitivity and selectivity. *Light:Science & Applications* **8**, 107 (2019).
15. Zhang, L. F. et al. A ZnO nanowire-based microfiber coupler for all-optical photodetection applications. *Nanoscale* **11**, 8319-8326 (2019).
16. Yang, L. Y. et al. Highly sensitive and miniature microfiber-based ultrasound sensor for photoacoustic tomography. *Opto-Electronic Advances* **5**, 200076 (2022).
17. Sagué, G. et al. Cold-atom physics using ultrathin optical fibers: light-induced dipole forces and surface interactions. *Physical Review Letters* **99**, 163602 (2007).
18. Solano, P. et al. Super-radiance reveals infinite-range dipole interactions through a nanofiber. *Nature Communications* **8**, 1857 (2017).
19. Lamsal, H. P., Franson, J. D. & Pittman, T. B. Transmission characteristics of optical nanofibers in metastable xenon. *Applied Optics* **58**, 6470-6473 (2019).
20. Gu, F. X. et al. Single whispering-gallery mode lasing in polymer bottle microresonators via spatial pump engineering. *Light:Science & Applications* **6**, e17061 (2017).
21. Ding, Z. X. et al. All-fiber ultrafast laser generating gigahertz-rate pulses based on a hybrid plasmonic microfiber resonator. *Advanced Photonics* **2**, 026002 (2020).
22. Nayak, K. P. et al. Optical nanofiber as an efficient tool for manipulating and probing atomic fluorescence. *Optics Express* **15**, 5431-5438 (2007).
23. She, W. L., Yu, J. H. & Feng, R. H. Observation of a push force on the end face of a nanometer silica filament exerted by outgoing light. *Physical Review Letters* **101**, 243601 (2008).
24. Cheng, C. et al. Surface enhanced Raman scattering of gold nanoparticles aggregated by a gold-nanofilm-coated nanofiber. *Photonics Research* **6**, 357-362 (2018).
25. Fujiwara, H. et al. Optical selection and sorting of nanoparticles according to quantum mechanical properties. *Science Advances* **7**, eabd9551 (2021).
26. Tong, L. M. Micro/nanofibre optical sensors: challenges and prospects. *Sensors* **18**, 903 (2018).
27. Sumetsky, M., Dulashko, Y. & Hale, A. Fabrication and study of bent and coiled free silica nanowires: self-coupling microloop optical interferometer. *Optics Express* **12**, 3521-3531 (2004).
28. Ward, J. M. et al. Contributed Review: optical micro- and nanofiber pulling rig. *Review of Scientific Instruments* **85**, 111501 (2014).
29. Hoffman, J. E. et al. Rayleigh scattering in an optical nanofiber as a probe of higher-order mode propagation. *Optica* **2**, 416-423 (2015).
30. Xu, Y. X., Fang, W. & Tong, L. M. Real-time control of micro/nanofiber waist diameter with ultrahigh accuracy and precision. *Optics Express* **25**, 10434-10440 (2017).
31. Chen, J. et al. Real-time measurement and control of nanofiber diameters using a femtowatt photodetector. *Optics Express* **30**, 12008-12013 (2022).
32. Jia, Q. N. et al. Fibre tapering using plasmonic microheaters and deformation-induced pull. *Light:Advanced Manufacturing* **4**, 5 (2023).
33. Hoffman, J. E. et al. Ultrahigh transmission optical nanofibers. *AIP Advances* **4**, 067124 (2014).
34. Kang, Y. et al. Ultrahigh-precision diameter control of nanofiber using direct mode cutoff feedback. *IEEE Photonics Technology Letters* **32**, 219-222 (2020).
35. Huang, K. J., Yang, S. Y. & Tong, L. M. Modeling of evanescent coupling between two parallel optical nanowires. *Applied Optics* **46**, 1429-1434 (2007).
36. Yu, X. C. et al. Single nanoparticle detection and sizing using a nanofiber pair in an aqueous environment. *Advanced Materials* **26**,

7462-7467 (2014).
37. Kien, F. L. et al. Coupling between guided modes of two parallel nanofibers. *New Journal of Physics* **22**, 123007 (2020).
38. Shao, L. Q. et al. Twin-nanofiber structure for a highly efficient single-photon collection. *Optics Express* **30**, 9147-9155 (2022).
39. Shao, L. Q. et al. Experimental demonstration of a compact variable single-mode fiber coupler based on microfiber. *IEEE Photonics Technology Letters* **33**, 687-690 (2021).
40. Daly, M. et al. Nanostructured optical nanofibres for atom trapping. *New Journal of Physics* **16**, 053052 (2014).
41. Ke, Y. G. et al. Topological phase transitions and Thouless pumping of light in photonic waveguide arrays. *Laser & Photonics Reviews* **10**, 995-1001 (2016).
42. Zhang, L. et al. Ultrasensitive skin-like wearable optical sensors based on glass micro/nanofibers. *Opto-Electronic Advances* **3**, 190022 (2020).
43. Ma, S. Q. et al. Optical micro/nano fibers enabled smart textiles for human–machine interface. *Advanced Fiber Materials* **4**, 1108-1117 (2022).
44. Cen, Q. Q. et al. Microtaper leaky-mode spectrometer with picometer resolution. *eLight* **3**, 9 (2023).
45. Paek, U. C., Schroeder, C. M. & Kurkjian, C. R. Determination of the viscosity of high silica glasses during fibre drawing. *Glass Technology* **29**, 263-266 (1988).
46. Choudhury, S. R. & Jaluria, Y. Practical aspects in the drawing of an optical fiber. *Journal of Materials Research* **13**, 483-493 (1998).
47. Paek, U. C. & Runk, R. B. Physical behavior of the neck-down region during furnace drawing of silica fibers. *Journal of Applied Physics* **49**, 4417-4422 (1978).
48. Wei, Z. Y. et al. Free surface flow in high speed fiber drawing with large-diameter glass preforms. *Journal of Heat Transfer* **126**, 713-722 (2004).
49. Hoffmann, P., Dutoit, B. & Salathé, R. P. Comparison of mechanically drawn and protection layer chemically etched optical fiber tips. *Ultramicroscopy* **61**, 165-170 (1995).
50. Valaskovic, G. A., Holton, M. & Morrison, G. H. Parameter control, characterization, and optimization in the fabrication of optical fiber near-field probes. *Applied Optics* **34**, 1215-1228 (1995).
51. Lazarev, A. et al. Formation of fine near-field scanning optical microscopy tips. *Part II. By laser-heated pulling and bending. Review of Scientific Instruments* **74**, 3684-3688 (2003).
52. Xue, S. C. et al. Theoretical, numerical, and experimental analysis of optical fiber tapering. *Journal of Lightwave Technology* **25**, 1169-1176 (2007).
53. Ding, L. et al. Ultralow loss single-mode silica tapers manufactured by a microheater. *Applied Optics* **49**, 2441-2445 (2010).
54. Ma, C. J. et al. Design and fabrication of tapered microfiber waveguide with good optical and mechanical performance. *Journal of Modern Optics* **61**, 683-687 (2014).
55. Angell, C. A. Perspective on the glass transition. *Journal of Physics and Chemistry of Solids* **49**, 863-871 (1988).
56. Lee, S. H. K. & Jaluria, Y. Effects of variable properties and viscous dissipation during optical fiber drawing. *Journal of Heat Transfer* **118**, 350-358 (1996).
57. Vu, A. T. et al. Modeling of thermo-viscoelastic material behavior of glass over a wide temperature range in glass compression molding. *Journal of the American Ceramic Society* **103**, 2791-2807 (2020).
58. Schnaas, A. & Grabke, H. J. High-temperature corrosion and creep of Ni-Cr-Fe alloys in carburizing and oxidizing environments. *Oxidation of Metals* **12**, 387-404 (1978).
59. Kodentsov, A. A. et al. High-temperature nitridation of Ni-Cr alloys. *Metallurgical and Materials Transactions A* **27**, 59-69 (1996).